

Novel triphenylamine-based cyclometalated platinum(II) complexes for efficient luminescent oxygen sensing

Chun Liu*, Xinlong Song, Xiaofeng Rao, Yang Xing, Zhonggang Wang, Jianzhang Zhao, Jieshan Qiu

State Key Laboratory of Fine Chemicals, Dalian University of Technology, Linggong Road 2, Dalian 116024, China



ARTICLE INFO

Article history:

Received 16 August 2013

Received in revised form

18 September 2013

Accepted 19 September 2013

Available online 4 October 2013

Keywords:

Phosphorescence

Luminescence

Oxygen sensor

Platinum

Triphenylamine

Ligand-free Suzuki reaction

ABSTRACT

Novel triphenylamine-based cyclometalated Pt(II) complexes containing a pyridyl moiety have been synthesized and fully characterized. The cyclometalating ligands were prepared via an efficient palladium-catalyzed ligand-free Suzuki reaction of 4-(diphenylamino)phenylboronic acid with 2-pyridyl bromides under aerobic and aqueous conditions. The photophysical properties of the complexes exhibited that introducing an electron-withdrawing group like trifluoromethyl or cyano group on the 5-position of the pyridine ring affected the LUMO level of the Pt(II) complex significantly, resulting in a marked decrease in energy gap. Moreover, the complex with a cyano group at the 5-position imparts a substantial red-shift up to 56 nm. The O₂ sensitivity of the complexes was quantitatively evaluated in a polymer film. The results of the O₂-sensing sensitivity of the Pt(II) complexes demonstrated that the complex with a nitrile ligand exhibited the highest sensitivity ($K_{SV}^{O_2} = 0.102 \text{ Torr}^{-1}$). The triphenylamine-based cyclometalated Pt(II) complexes are potential candidates for efficient luminescent oxygen sensing.

© 2013 Elsevier Ltd. All rights reserved.

1. Introduction

Luminescence oxygen sensors have potential application in a variety of fields, such as chemical industry, clinical analysis, environmental monitoring, oceanography, and biology [1–9]. One of the main composes of an oxygen sensor is the transition-metal complex, which is usually immobilized on a polymer film [10–12] and acts as an oxygen sensitizer because oxygen diffuses from the surrounding medium into the film and plays a role as a powerful quencher of the electronically excited state of the metal complex [11]. In 1985, a new optical method based on phosphorescence lifetime quenching was used for the measurement of oxygen in biological systems [13]. The photophysical and photochemical properties of phosphorescent transition-metal complexes with a long lifetime in the range of microseconds including cyclometalated Ru(II), Ir(III), and Pt(II) complexes are ideal for luminescence O₂ sensing [5,14–16]. Ruthenium-tris(dipyridyl)dichloride is the first reported Ru(II) complex for oxygen sensor with an indicator embedded in silica [17]. In 1996, Marco and co-workers reported the first use of an Ir(III) complex as the active species in the luminescence oxygen sensor [18]. Luminescent Pt(II) complexes have also attracted much

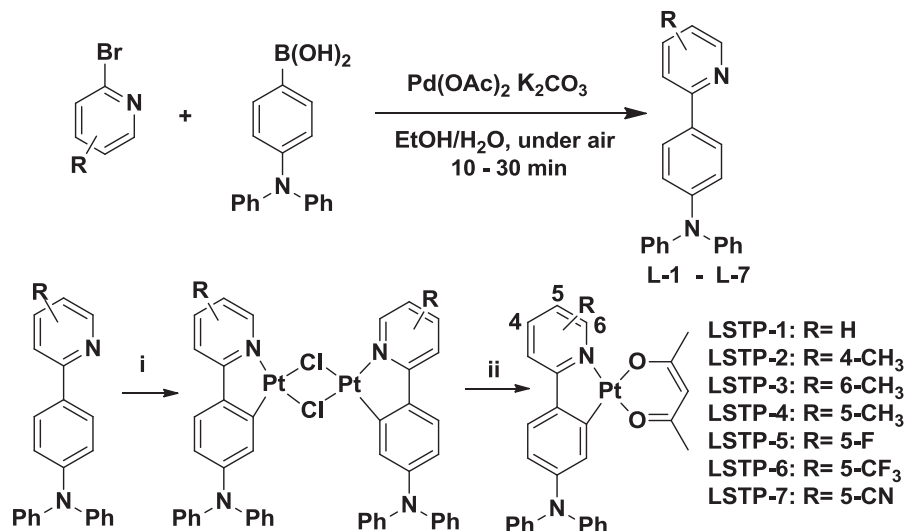
attention since they may be potentially used as advanced functional materials for organic light-emitting devices (OLEDs), dye-sensitized solar cells, oxygen sensors, and photoreceptors in biological molecules [19–28]. In 1991, the Pt(II) complexes were first applied for the fiber-optic oxygen sensor [29]. Although a variety of Pt(II) complexes with porphyrin ligands found application in optical sensors [10,30–32], only few Pt(II) complexes from other cyclometalating ligands were reported [33].

Triphenylamine (TPA) derivatives, due to the non-coplanarity of the three phenyl substituents, strong electron-donating nature, good hole-transporting capability and high light-to-electrical energy-conversion efficiency, are important structural motifs in numerous organic electroluminescence materials [34–39]. In 2009, Chan and co-workers reported the first use of Ir(ppy-NPh₂)₃ complex for luminescence oxygen sensing [40]. Later, Zhao et al. synthesized Pt(ppy-NPh₂)(acac) complex, which was the first example of a Pt(II) complex containing a TPA moiety for oxygen sensing [16]. To the best of our knowledge, no report on the structure–function relationship of Pt complex with a substituent at the pyridyl ring of the ppy-NPh₂ cyclometalating ligand has been described in the literature. Therefore, further investigation is necessary to elucidate the merits of TPA-based cyclometalated Pt(II) complexes for oxygen sensing.

In the present paper, we describe the synthesis, structures and photoelectric performances of novel cyclometalated platinum

* Corresponding author. Tel.: +86 411 84986182.

E-mail address: chunliu70@yahoo.com (C. Liu).



Scheme 1. Structures of the cyclometalated Pt(II) complexes featuring triphenylamine derivatives. i) K_2PtCl_4 , 2-ethoxyethanol/water (3:1, v/v), N_2 , 100 °C, 24 h; ii) $Hacac$, Na_2CO_3 , 2-ethoxyethanol, N_2 , 100 °C, 24 h.

complexes with 4-(2-pyridyl)- substituted TPA derivatives (**Scheme 1**). The TPA derivatives used in this study were prepared efficiently via a palladium-catalyzed ligand-free and aerobic Suzuki reaction in aqueous ethanol developed by our group recently [41], which will be used to investigate the relationship of structure–photoelectric properties of the novel Pt(II) complexes and to evaluate the performances in oxygen sensing.

2. Experimental

2.1. Materials and instruments

All the cross-coupling reactions for preparing the ligands were carried out in air. 2-Bromopyridines were purchased from Alfa Aesar. 4-(Diphenylamino) phenylboronic acid was purchased from Trusyn Chem-Tech Co., Ltd., China. Other chemicals were purchased from commercial sources and used without further purification. 1H NMR and ^{13}C NMR spectra were recorded on a 400 MHz Varian Unity Inova spectrophotometer. Mass spectra were recorded with a MALDI micro MX spectrometer. The intensities of the crystal data were collected on a Bruker SMART APEX II CCD diffractometer with graphite-monochromated Mo-K α ($\lambda = 0.71073 \text{ \AA}$) using the SMART and SAINT programs. UV/Vis absorption spectra were recorded on an HP8453 UV/Vis spectrophotometer. Fluorescence spectra were recorded with a PTI-700 spectrofluorimeter. Luminescent quantum yields were measured with $[Ir(ppy)_3]$ ($UP = 0.40$, $\lambda_{ex} = 400 \text{ nm}$, in CH_2Cl_2 , under degassed conditions). Phosphorescence lifetimes were measured on an Edinburgh FLS920 Spectrometer in a degassed dichloromethane solution with excitation wavelength at 410 nm. Cyclic voltammograms of the Pt(II) complexes were recorded on an electrochemical workstation (BAS100B/W, USA) at room temperature in a 0.1 M $[Bu_4N]PF_6$ solution under nitrogen gas protection.

2.2. Synthesis of the cyclometalated Pt(II) complexes

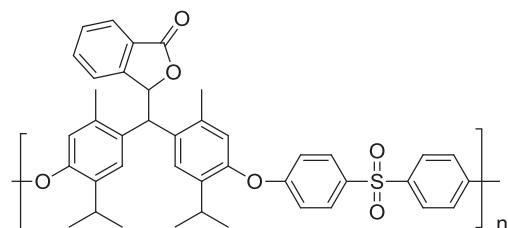
Cyclometalating ligands with a TPA moiety L-1–L-7 were synthesized according to an efficient ligand-free Suzuki reaction [41], which were then used to synthesize new Pt(II) complexes via two distinctive steps as previously reported (**Scheme 1**) [42]. Synthetic procedure of cyclometalating ligands L-1–L-7: a mixture of 2-pyridyl bromide (0.25 mmol), 1.5 equiv of 4-(diphenylamino)

phenylboronic acid (0.375 mmol, 0.108 g), 2 equiv of K_2CO_3 (0.5 mmol, 0.069 g), $Pd(OAc)_2$ (1.5 mol%, 0.00375 mmol, 0.84 mg), ethanol/water (3 mL/1 mL) was stirred at 80 °C in air for indicated time. The reaction mixture was added to brine (15 mL) and extracted four times with ethyl acetate (4 × 15 mL). The solvent was concentrated and the product was isolated by short-column chromatography. The cyclometalating ligand was reacted with 1.2 equiv K_2PtCl_4 (0.2 mmol, 83.02 mg) in a mixture of 2-ethoxyethanol and water (6 mL/2 mL) at 80 °C for 16–24 h to afford a platinum dimer, which was subsequently reacted with 5 equiv of the chelating diketone (0.1 mmol, 102.5 μL) and 10 equiv of Na_2CO_3 (1 mmol, 0.106 g) in 2-ethoxyethanol at 100 °C for 18–24 h.

LSTP-1 [39]. Eluent: CH_2Cl_2 /hexane (1:1, v/v). A yellow solid; yield: 70.2%. 1H NMR (400 MHz, $CDCl_3$): $\delta = 8.87$ (d, $J = 5.2 \text{ Hz}$, 1H, Py), 7.71 (t, $J = 7.7 \text{ Hz}$, 1H, Ph), 7.47 (d, $J = 7.8 \text{ Hz}$, 1H, Py), 7.24–7.29 (m, 5H, Py and Ph), 7.18–7.24 (m, 5H, Ph), 6.97–7.05 (m, 3H, Ph), 6.76 (d, $J = 8.4 \text{ Hz}$, 1H, Ph), 5.38 (s, 1H, CH), 1.96 (s, 3H, CH_3), 1.72 (s, 3H, CH_3).

LSTP-2. Eluent: CH_2Cl_2 /hexane (3:1, v/v). A yellow solid; yield: 38.4%; 1H NMR (400 MHz, $CDCl_3$): $\delta = 8.67$ (d, $J = 6.0 \text{ Hz}$, 1H, Py), 7.26–7.27 (m, 2H, Ph), 7.21–7.24 (m, 2H, Py), 7.00–7.20 (m, 5H, Ph), 6.80–7.00 (m, 4H, Ph), 6.76 (d, $J = 6.8 \text{ Hz}$, 1H, Ph), 6.74 (dd, $J = 2.3 \text{ Hz}$, 1H, Ph), 5.37 (s, 1H, CH), 2.40 (s, 3H, CH_3), 1.95 (s, 3H, CH_3), 1.70 (s, 3H, CH_3). ^{13}C NMR (100 MHz, $CDCl_3$): $\delta = 185.50$, 183.97 (CO), 167.18, 149.59, 148.16, 147.59, 146.41, 139.70, 138.23, 129.19, 129.06, 124.16, 123.64, 123.25, 120.99, 118.32, 117.62 (Ar), 102.24 (CH), 28.23, 26.82, 21.57 (CH_3). HRMS (EI): calcd. for $C_{29}H_{26}N_2O_2Pt$ [M]⁺ 629.1642; found: 629.1655.

LSTP-3. Eluent: CH_2Cl_2 /hexane (3:1, v/v). A yellow solid; Yield: 27.8%. 1H NMR (400 MHz, $CDCl_3$): $\delta = 7.53$ (t, $J = 7.8 \text{ Hz}$, 1H, Py), 7.25–7.32 (m, 4H, Ph), 7.18–7.25 (m, 7H, Py and Ph), 7.02 (t,



Scheme 2. The structure of polymer IMPES-C for this study.

$J = 7.2$ Hz, 2H, Ph), 6.81 (d, $J = 7.0$ Hz, 1H, Ph), 6.75 (dd, $J = 8.4$ Hz, 1H, Ph), 5.39 (s, 1H, CH), 2.91 (s, 3H, CH₃), 1.88 (s, 3H, CH₃), 1.62 (s, 3H, CH₃). ¹³C NMR (100 MHz, CDCl₃): δ = 185.36, 183.51 (CO), 168.82, 163.19, 147.56, 147.41, 139.28, 137.42, 137.28, 129.08, 125.53, 123.77, 123.13, 122.04, 121.90, 117.56, 114.67 (Ar), 101.33 (CH), 28.01,

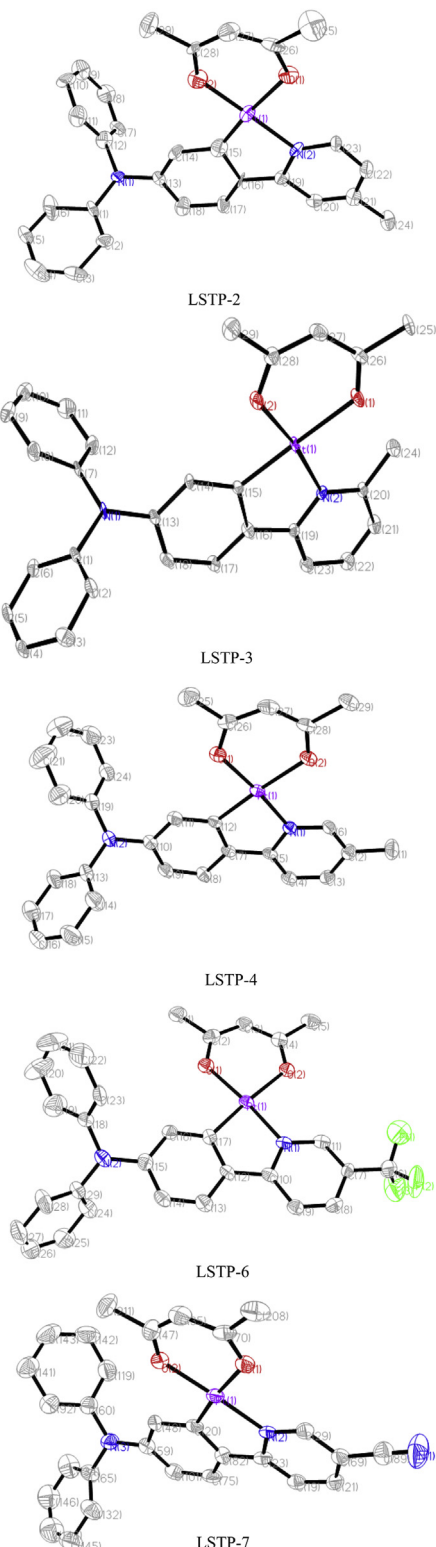


Fig. 1. Perspective view of the crystal structure of Pt(II) complexes (30% probability ellipsoids, hydrogen atom labels have been omitted for clarity).

26.58, 24.87 (CH₃). HRMS (EI): calcd. for C₂₉H₂₆N₂O₂Pt [M]⁺ 629.1642; found: 629.1620.

LSTP-4. Eluent: CH₂Cl₂/hexane (3:1, v/v). A yellow solid; Yield: 41.6%. ¹H NMR (400 MHz, CDCl₃): δ = 8.68 (s, 1H, Py), 7.55 (d, $J = 7.8$ Hz, 1H, Ph), 7.37 (d, $J = 8.3$ Hz, 1H, Py), 7.26–7.35 (m, 6H, Ph), 7.17–7.20 (m, 4H, Py and Ph), 7.01–7.03 (t, $J = 7.2$ Hz, 2H, Ph), 6.75 (dd, $J = 8.4$ Hz, 1H, Ph), 5.38 (s, 1H, CH), 2.36 (s, 3H, CH₃), 1.97 (s, 3H, CH₃), 1.71 (s, 3H, CH₃). ¹³C NMR (100 MHz, CDCl₃): δ = 185.60, 184.04 (CO), 165.15, 147.86, 147.64, 146.85, 139.07, 138.76, 138.49, 129.98, 129.07, 125.26, 123.42, 123.38, 122.97, 117.82, 117.28 (Ar), 102.29 (CH), 28.31, 26.83, 18.20 (CH₃). HRMS (EI): calcd. for C₂₉H₂₆N₂O₂Pt [M]⁺ 629.1642; found: 629.1592.

LSTP-5. Eluent: CH₂Cl₂/hexane (3:1, v/v). A yellow solid; Yield: 40.6%. ¹H NMR (400 MHz, CDCl₃): δ = 8.82 (s, 1H, Py), 7.54 (m, 1H, Ph), 7.44 (m, 1H, Ph), 7.26–7.28 (m, 2H, Py), 7.20–7.25 (m, 8H, Ph), 7.03–7.17 (t, $J = 7.2$ Hz, 2H, Ph), 6.76 (d, $J = 8.4$ Hz, 1H, Ph), 5.39 (s, 1H, CH), 1.97 (s, 3H, CH₃), 1.72 (s, 3H, CH₃). ¹³C NMR (100 MHz, CDCl₃): δ = 185.90, 184.13 (CO), 164.79, 157.53, 155.06, 148.36, 147.45, 138.96, 136.93, 135.70, 135.38, 129.12, 125.53, 125.46, 125.34, 123.84, 123.23, 123.03, 118.12, 118.06, 117.55 (Ar), 102.42 (CH), 28.23, 26.75 (CH₃). HRMS (EI): calcd. for C₂₈H₂₃N₂O₂PtF [M – H]⁻ 632.1313; found: 632.1341.

LSTP-6. Eluent: CH₂Cl₂/hexane (3:1, v/v). A yellow solid; Yield: 50.3%. ¹H NMR (400 MHz, CDCl₃): δ = 9.14 (s, 1H, Py), 7.86 (dd, $J = 8.6$ Hz, 1H, Ph), 7.50 (d, $J = 8.6$ Hz, 1H, Ph), 7.25–7.31 (m, 5H, Py and Ph), 7.17–7.25 (m, 5H, Ph), 7.06–7.10 (m, 3H, Ph), 6.75 (dd, $J = 8.5$ Hz, 1H, Ph), 5.40 (s, 1H, CH), 1.98 (s, 3H, CH₃), 1.71 (s, 3H, CH₃). ¹³C NMR (100 MHz, CDCl₃): δ = 186.09, 184.10 (CO), 170.95, 149.82, 147.00, 144.39, 141.88, 135.37, 134.56, 129.24, 126.10 (Ar), 125.39 (CF₃), 123.90, 121.65, 117.10, 116.49, 103.82 (Ar), 102.40 (CH), 28.24, 26.71 (CH₃). HRMS (EI): calcd. for C₂₉H₂₃N₂O₂PtF₃ [M]⁻ 683.1359; found: 683.1378.

LSTP-7. Eluent: CH₂Cl₂/hexane (2:1, v/v). A red solid; Yield: 36.7%. ¹H NMR (400 MHz, CDCl₃): δ = 9.13 (s, 1H, Py), 7.85 (d, $J = 8.4$ Hz, 1H, Ph), 7.32 (d, $J = 8.9$ Hz, 1H, Py), 7.29 (s, 1H, Ph), 7.20–7.25 (m, 7H, Py and Ph), 7.11–7.20 (m, 4H, Ph), 6.74 (d, $J = 14.8$ Hz, 1H, Ph), 5.40 (s, 1H, CH), 2.00 (s, 3H, CH₃), 1.71 (s, 3H, CH₃). ¹³C NMR (100 MHz, CDCl₃): δ = 186.27, 184.16 (CO), 171.08, 150.52, 150.32, 146.66, 143.05, 139.81, 134.51, 129.31, 126.40, 124.32, 120.93, 117.09, 116.13, 116.09, 111.35 (Ar), 103.71 (CN), 102.51 (CH), 28.26, 26.67 (CH₃). HRMS (EI): calcd. for C₂₉H₂₃N₃O₂Pt [M]⁺ 640.1438; found: 640.1451.

2.3. Luminescent oxygen sensing

A home-assembled flow cell and optical fiber were used for the oxygen sensing. Typical oxygen film preparation is as follows. IMPES-C polymer ([Scheme 2](#)) (10.0 mg) prepared according to the literature [[7](#)] was dissolved in acetone (0.5 mL) and then the Pt complex in CH₂Cl₂ (0.2 mL, 1.0×10^{-3} mol dm⁻³) was added to the solution. After thoroughly mixing, about 0.3 mL of the solution was coated on a silica glass disk (diameter 1.6 cm). The solvent was evaporated at room temperature and a transparent film was obtained. The thickness of the film containing LSTP-1 was estimated to be 15.8 μ m from the weight of the film (6.1 mg) and the density of the polymer (1.21 g cm⁻³). The film thicknesses of the complexes LSTP-2–LSTP-7 were estimated by the same method to be 16.0, 17.3, 15.9, 16.3, 15.8, and 18.0 μ m, respectively.

3. Results and discussion

3.1. Crystal structures

To further establish their molecular structures, a majority of these Pt(II) complexes were subjected to X-ray single-crystal

Table 1

X-ray selected bond lengths (\AA) and angles ($^\circ$) around the metal core in the Pt(II) complexes.

	Pt–N	Pt–C	Pt–O	C–Pt–N	O–Pt–O	Pt–Pt
LSTP-1 [39]	1.9954	1.9574	2.0943 (2.0013)	81.56	92.04	3.394
LSTP-2	1.8835	1.9889	2.1238 (2.0195)	85.51	91.20	2.843
LSTP-3	2.0574	1.9623	2.1061 (1.9996)	81.27	88.57	3.865
LSTP-4	1.9952	1.9699	2.0850 (1.9946)	81.98	92.12	3.483
LSTP-6	1.9956	1.9436	2.0702 (1.9959)	81.95	92.19	4.904
LSTP-7	2.0013	1.9722	2.1007 (2.0026)	82.21	92.26	4.571

diffraction studies. All of them can rapidly form microcrystalline solids from solvent mixtures of trichloromethane and hexane. Perspective drawings of Pt(II) complexes are shown in Fig. 1. And key bonding parameters are given in Table 1. The Pt–N distance is 1.883(5)–2.057(4) \AA , which is slightly longer than that of common Pt–N bonds. The Pt–C distance is 1.943(6)–1.988(9) \AA . The C–Pt–N and O–Pt–O angles are 81.27–85.51 $^\circ$ and 88.57–92.26 $^\circ$, which are similar to reported values [39]. The bond distance of the Pt–O edge *trans* to C atom 2.070(2)–2.123(8) \AA is larger compared to that of the other Pt–O bond 1.994(6)–2.019(5) \AA . Because the O atom *trans* to C atom has a strong *trans* influence. The Pt···Pt distances in LSTP-1, 2 and 4 are in the range of 2.7–3.5 \AA and thus a weak Pt···Pt interaction are possible in the crystal. The Pt···Pt interaction don't exist in LSTP-3, 6 and 7. All other bond lengths around the Pt core are typical for cyclometalates and β -diketonate derivatives of Pt(II) [42–45].

3.2. Photophysical and thermal properties

Since good thermal stabilities of the compounds are very important for applications, the onset decomposition temperatures (T_{dec}) of the new compounds were determined from thermogravimetric analysis (TGA) under a nitrogen stream. It is clear from the onset of the TGA curves, all Pt(II) complexes exhibit high thermal stability with their T_{dec} ranging from 230 to 320 $^\circ\text{C}$ (Table 2). The first weight loss of the compounds was mostly due to dissociation of the ancillary acac ligand, which are necessary for high-performance oxygen sensors.

The absorption and emission data of the Pt(II) complexes LSTP-1–LSTP-7 are shown in Table 2. In common with all Pt(II) complexes the absorption spectra can be divided into two regions: the strong absorptions in the UV region (<350 nm) are derived from a typical ligand-centered π – π^* transition because the corresponding transitions were also observed in the free ligands. The second regions that extend to the visible region are conventionally assigned as mixing among singlet and triplet metal-to-ligand charge transfer transitions ($^1\text{MLCT}$ and $^3\text{MLCT}$) and to a certain extent with intra-ligand π – π^* transitions through the spin-orbit coupling by the

heavy metal center, which are not observed in the free ligands. It is likely that the strong ligand field of the cyclometalating ligands shifts the d–d transitions to high energy, putting them under the more intense ligand-centered (LC) transitions. The substituents on the N,N-diphenyl-4-(pyridin-2-yl)aniline have significant influence on the absorption properties of the complexes. The lower-lying band is shifted upon the attachment of different substituents on the pyridyl ring in the order: LSTP-7 ($\lambda_{\text{max}} = 474 \text{ nm}$) > LSTP-6 (451 nm) > LSTP-5 (427 nm) > (LSTP-1 (424 nm), LSTP-3 (422 nm), LSTP-4 (421 nm)) > LSTP-2 (415 nm). These results agree with the literature data that introduction of electron-withdrawing groups to the pyridine ring can cause a decrease of the HOMO level and a larger band gap than the unsubstituted one and vice versa. Fig. 2 shows the absorption spectra of LSTP-1–LSTP-7.

The room temperature phosphorescence spectra of LSTP-1–LSTP-7 are depicted in Fig. 2. The colors of the complexes span from green to yellow and orange (in the web version). Fig. 3 shows the color-tuning strategy achieved by the modification of the pyridyl ring of Pt(II) complexes with different substituents. The emission spectra possess distinctive vibronic like progression, which we can expect a significant amount of $^3\text{MLCT}$ state mixing with the ligand-centered $^3\pi$ – π transitions. The emission energies are strongly sensitive to the electronic properties of substituents on the pyridyl ring. A weakly donating methyl group at the 4-position of the pyridyl ring results in a slight blue-shift of 7 nm for LSTP-2 comparing to LSTP-1. The emission is not influenced by the methyl group in the 5- or 6-position at the pyridyl ring for LSTP-3 and LSTP-4. The stronger electron acceptor of trifluoromethyl group at the 5-position on the pyridyl ring imparts a substantial red-shift of 28 nm for LSTP-6, while the cyano group at the same position imparts a more substantial red-shift up to 56 nm for LSTP-7. A fluoro group in the 5-position causes a bathochromic shift of 9 nm for LSTP-5. Therefore, λ_{em} decreases in the following order: LSTP-7 > LSTP-6 > LSTP-5 > (LSTP-3, LSTP-4, LSTP-1) > LSTP-2.

We further probed the photophysical properties of LSTP-1–LSTP-7 by measuring their PL quantum yields (Φ_p) in dilute degassed CH_2Cl_2 solutions. Among all the green/yellow/orange (in the web version) compounds, LSTP-4 has the highest room temperature quantum efficiency of 19%, which is higher than that for its isomeric compound LSTP-2 (9%) and LSTP-3 (4%). An increase in Φ_p (16%) was observed when a trifluoromethyl group was attached to the pyridine ring. As the energy of emission decreases, a corresponding general decrease in Φ_p at room temperature is observed. We propose that the red-shifted emission is due to the strong electron-donating ability of the diphenylamine group.

3.3. Density functional theory (DFT) calculations

The structures of the complexes were optimized using density functional theory (DFT) [46] with the B3LYP functional and 6-31G(d)/LanL2DZ basis set. The 6-31G(d) basis set was employed

Table 2

Photophysical and thermal data for the Pt(II) complexes.

Compound	Absorption (293 K) λ_{abs} (nm) ^a CH_2Cl_2	Emission (293 K) λ_{em} (nm) CH_2Cl_2	Φ_p ^b	Γ (μs) ^c	T_{dec} ($^\circ\text{C}$)
LSTP-1	256 (1.50), 307 (1.01), 333 (0.93), 424 (0.84)	540, 578sh	0.11	5.11	290 [30]
LSTP-2	257 (1.97), 307 (1.43), 415 (1.15)	533, 572sh	0.09	12.22	270
LSTP-3	256 (1.90), 309 (1.48), 342 (1.46), 422 (1.10)	542, 585sh	0.04	13.90	230
LSTP-4	239 (1.43), 257 (1.44), 312 (0.91), 421 (0.69)	541, 580sh	0.19	6.96	290
LSTP-5	256 (1.84), 308 (1.19), 346 (1.18), 427 (0.70)	549, 590sh	0.11	6.43	250
LSTP-6	257 (2.17), 303 (1.23), 358 (1.03), 451 (1.47)	568	0.14	9.08	320
LSTP-7	257 (2.38), 287 (1.70), 369 (0.99), 474 (2.30)	595	0.03	10.94	290

^a Extinction coefficients ($10^4 \text{ M}^{-1} \text{ cm}^{-1}$) are shown in parentheses.

^b Phosphorescence quantum yield in degassed dichloromethane. Measured in dichloromethane relative to $[\text{Ir}(\text{ppy})_3]$ (UP = 0.40), $\lambda_{\text{ex}} = 400 \text{ nm}$.

^c In degassed dichloromethane, 25 $^\circ\text{C}$.

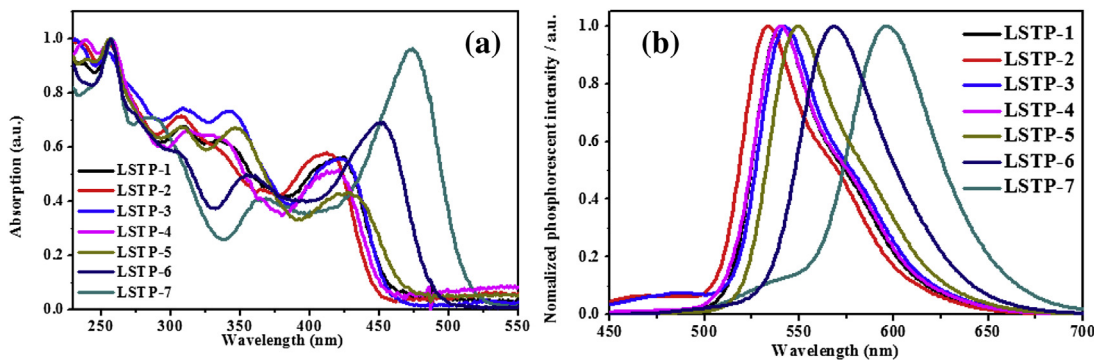


Fig. 2. (a) Absorption spectra and PL spectra of the Pt(II) complexes; $c = 1.0 \times 10^{-5}$ mol dm $^{-3}$ in degassed dichloromethane. 25 °C.

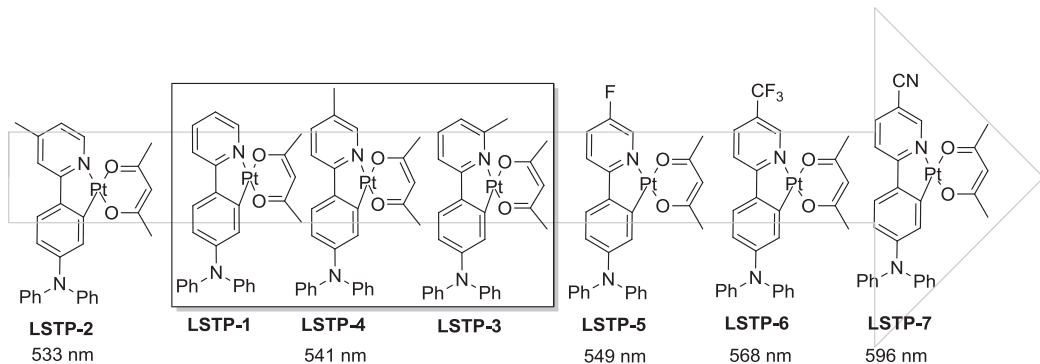
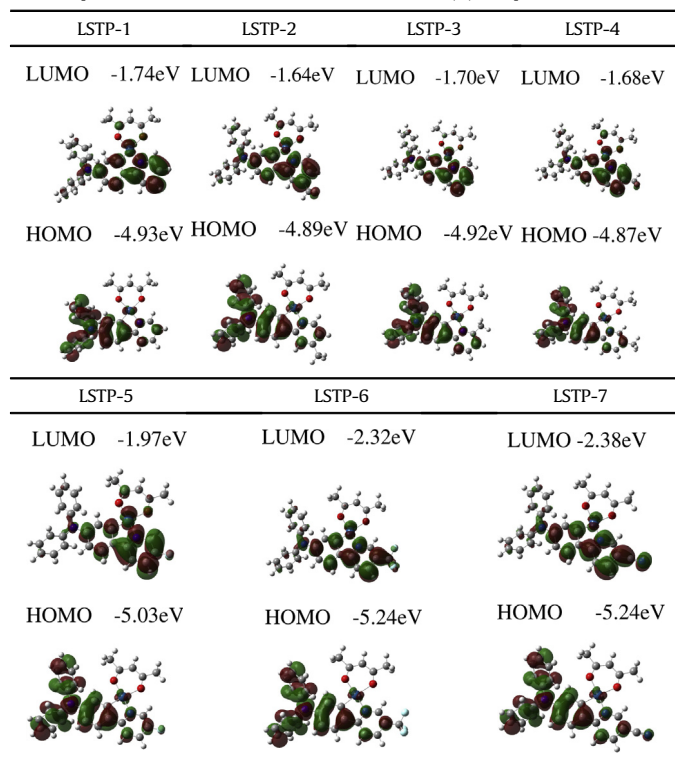


Fig. 3. Color-tuning strategy in cyclometalated Pt(II) complexes.

for C, H, N, O and the LanL2DZ basis set was used for Pt(II). All these calculations were performed with the Gaussian 09 software package [47]. To study the electronic structures and understand the nature of excited states of our new Pt(II) phosphors, density

Table 3

Contour plots of dominant excitation orbitals of the Pt(II) complexes.



functional theory (DFT) calculations were carried out using B3LYP hybrid functional theory for selected molecules. From Table 3, it is clear that the HOMO–LUMO gaps calculated for LSTP-1–LSTP-4 are close to each other, revealing that the HOMO and LUMO levels are not influenced by a weakly σ -donating methyl group in the 6-position or 5-position on the pyridyl ring. In contrast, the HOMO and LUMO levels are little influenced by the 4, 5, 6-methyl or 5-fluoro on the pyridyl ring. Introducing an electron-withdrawing cyano or trifluoromethyl group on the pyridine ring affects the LUMO level significantly, resulting in a marked decrease in energy gap.

3.4. Electrochemical and electronic characterization

The electrochemical properties of LSTP-1–LSTP-7 were examined using cyclic voltammetry, and the redox data are given in Table 4. All of the electrochemical potentials reported here were measured relative to an internal ferrocene standard ($\text{Cp}_2\text{Fe}/\text{Cp}_2\text{Fe}^+$) [48]. All Pt(II) complexes show reversible reduction and irreversible oxidation waves. This electrochemical behavior is

Table 4

Electrochemical properties and frontier orbital energy levels of the Pt(II) complexes.

Compound	HOMO (eV) ^a	LUMO (eV) ^b	Eg (eV) ^c
LSTP-1	-5.02	-1.73	3.29
LSTP-2	-4.91	-1.69	3.22
LSTP-3	-4.91	-1.73	3.18
LSTP-4	-5.05	-1.74	3.31
LSTP-5	-5.35	-2.25	3.10
LSTP-6	-5.39	-2.42	2.97
LSTP-7	-5.37	-2.51	2.86

^a 0.1 M $[\text{Bu}_4\text{N}]^+\text{PF}_6^-$ in CH_2Cl_2 , scan rate 100 mV s $^{-1}$, versus Fc/Fc^+ couple.

^b LUMO = HOMO + Eg.

^c Estimated from the absorption edge (λ_{edge}) of solid films by equation of $\text{Eg} = 1240/\lambda_{\text{edge}}$.

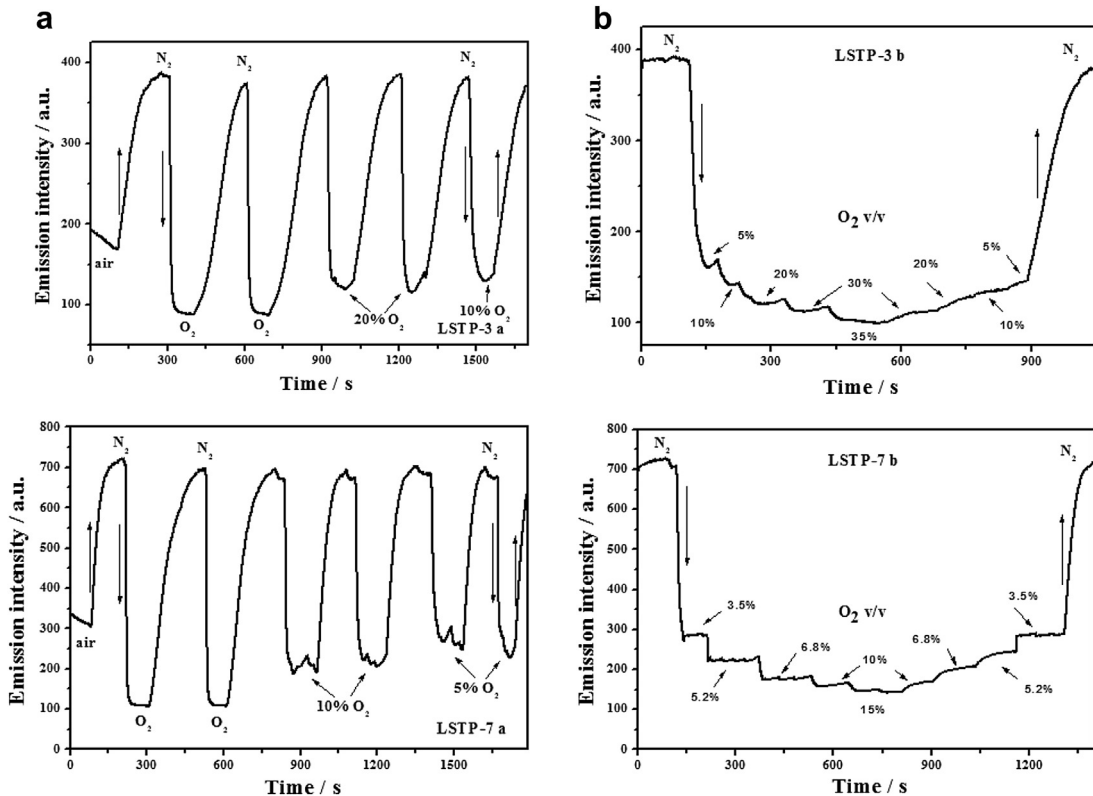


Fig. 4. Phosphorescent intensity response of sensing films of the complexes in IMPES-C to saturation O₂/N₂ cycles and small-step variations of O₂ concentrations. (a) Saturation switching emissive intensity response of sensing films of LSTP-3, LSTP-7 in IMPES-C to O₂/N₂ saturation cycles. (b) Dynamic emissive intensity response of sensing films of LSTP-3, LSTP-7 in IMPES-C to O₂/N₂ saturation cycles, 25 °C.

similar to that reported for related Pt(II) complexes [49]. According to the results in Tables 3 and 4, the LUMO level is predominantly pyridyl in character, while the HOMO level is mainly influenced by the triphenylamine unit. This is mainly attributed to the poorer electron-accepting property of triphenylamine as compared to the phenyl ring. The results in Table 4 demonstrated that the reduction potentials of these complexes are strongly sensitive to the nature of substituents on the pyridyl ring. When an electron-donating group (such as 4, 5, or 6-methyl group) is attached to the pyridyl ring, the LUMO level is close to each other. On the other hand, addition of an electron-withdrawing substituent, such as cyano group (LSTP-7), fluorine (LSTP-5) or trifluoromethyl group (LSTP-6), reduces the LUMO level. Therefore, the LUMO level decreases in the order of LSTP-2 (-1.69 eV) > LSTP-1 (-1.73 eV), LSTP-3 (-1.73 eV), LSTP-4 (-1.74 eV) > LSTP-5 (-2.25 eV) > LSTP-6 (-2.42 eV) > LSTP-7 (-2.51 eV). This is in agreement with the results described in literature [49–51] and a red-shift in the emission wavelength often occurs when lowering the LUMO energy level.

As compared to Pt(ppy)acac (HOMO: -5.34 eV) [42], the HOMO levels of LSTP-1–LSTP-7 are all elevated when the electron-rich triphenylamine unit are attached to the pyridyl rings, signaling that they have a lower ionization potential than ppy, leading to a better hole-injection (HI) and/or hole-transporting (HT) ability.

3.5. Luminescent O₂ sensing of the Pt(II) complexes in polymer films

For practical application of a metal complex as an indicator for O₂ sensing, the study of sensing films prepared by the distribution of metal complexes in supporting polymers is more meaningful than the study in a solution [2,16,52,53].

Thus, the O₂-sensing properties of the as-prepared complexes were studied in polymer films (IMPES-C). Fig. 4 demonstrates the phosphorescent intensity responses of sensing films of the complexes LSTP-3 and LSTP-7 in IMPES-C to saturation O₂/N₂ cycles and small-step variations of O₂ concentrations.

The Stern–Volmer quenching equation (Eq. (1)) is used to quantitatively describe the luminescence O₂ sensing [2].

$$\frac{I_0}{I} = \frac{\tau_0}{\tau} = 1 + k_q \tau_0 [Q] \quad (1)$$

where I_0 stands for the emission intensity in inert atmosphere (nitrogen for this study), I is the emission intensity under specific

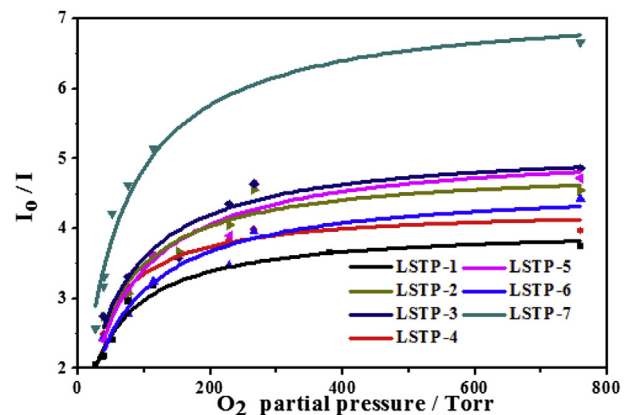


Fig. 5. Two-site model plots for the sensing films of the Pt(II) complexes in IMPES-C. Intensity ratios I_0/I versus O₂ partial pressure.

Table 5

Parameters for the O₂-sensing film of the Pt(II) complexes with IMPES-C as the supporting matrix (fitting of the results to the two-site model).

	λ_{ex} (nm)	λ_{em} (nm)	f_{01}^{a}	f_{02}^{a}	$K_{\text{SV1}}^{\text{b}}$	$K_{\text{SV2}}^{\text{b}}$	$r^2 \text{c}$	$K_{\text{SV}}^{\text{app}} \text{d}$	$p\text{O}_2^{\text{e}}$
LSTP-1	425	542	0.7509	0.2491	0.0761	0.000	0.971	0.05714	23.4
LSTP-2	420	533	0.7673	0.2327	0.1069	0.000	0.936	0.08202	17.9
LSTP-3	425	542	0.7840	0.2160	0.0647	0.000	0.931	0.05072	26.6
LSTP-4	425	541	0.8067	0.1933	0.0713	0.001	0.935	0.05752	24.6
LSTP-5	430	549	0.7955	0.2045	0.0871	0.001	0.907	0.06929	21.9
LSTP-6	455	569	0.8074	0.1926	0.0833	0.000	0.913	0.06726	22.6
LSTP-7	475	596	0.8616	0.1384	0.1180	0.001	0.966	0.10167	9.7

^a Ratio of the two portions of the Pt(II) complexes.

^b Quenching constants of the two portions.

^c Determination coefficients.

^d Weighted quenching constant, $K_{\text{SV}}^{\text{app}} = f_{01}K_{\text{SV1}} + f_{02}K_{\text{SV2}}$.

^e The oxygen partial pressure at which the initial emission intensity of the film is quenched by 50% and calculated as $1/K_{\text{SV}}$, in Torr.

O₂ partial pressure, k_q is the quenching constant, τ_0 is the unquenched lifetime and [Q] is the concentration of the quencher.

For heterogenous O₂-sensing films, a modified Stern–Volmer or a two-site model is required to study the quenching effect [7,54]. In the two-site model, the O₂-sensitive complexes are considered as two different portions. Because even in “homogeneous” polymers, the complexes still dwell in different microenvironments [40,52]. The fraction of the two portions are defined as f_{01} and f_{02} , respectively ($f_{01} + f_{02} = 1$); the two portions have different quenching constants (K_{SV1} and K_{SV2}); see Eq. (2).

$$\frac{I_0}{I} = \left(\frac{f_{01}}{1 + K_{\text{SV1}}[\text{O}_2]} + \frac{f_{02}}{1 + K_{\text{SV2}}[\text{O}_2]} \right)^{-1} \quad (2)$$

With the home-assembled flow cell coupled to a spectrofluorimeter, the responses of the sensing films to different O₂ partial pressure were studied (Fig. 4). First the O₂-sensing films of LSTP-3 and LSTP-7 were tested against the saturation cycle of O₂ and N₂ (Fig. 4, LSTP-3a and LSTP-7a) (others see the Supporting information). The films in N₂ exhibit intense emission, but the phosphorescence is substantially quenched in O₂. Furthermore, fast response ($t \downarrow 90$) and recovery times ($t \uparrow 90$) of 5–10 s and 20–30 s were observed, respectively [15,54]. The response ($t \downarrow 90$) and recovery times ($t \uparrow 90$) are generally accepted as the times for luminescence intensity changes to reach 90% of the whole variation when switching from 100% N₂ to 100% O₂ or vice versa. Fast response times are usually observed for porous supporting materials such as MCM-41 molecular sieves [19,55–59]. Next, the dynamic response of the O₂-sensing films was tested against small steps of O₂ partial pressure variation (Fig. 4, LSTP-3b and LSTP-7b) (others see the Supporting information). Such a detailed study will reveal the dynamic O₂ partial pressure range and the data can be used to evaluate the O₂ sensitivity. We found that the sensing film with LSTP-7 is more sensitive to O₂ than others. For example, the emission intensity of LSTP-7 was quenched by 69.7% under 3.5% O₂. For others, however, the emission is quenched by only around (54–60)% in the presence of 5% O₂. To compare the O₂-sensing properties of the complexes quantitatively, the O₂-sensing data were fitted to the two-site model (Fig. 5) and the results are summarized in Table 5. The $K_{\text{SV}}^{\text{app}}$ value is not influenced by a methyl group in the 5-position or 6-position on the pyridyl ring comparing to LSTP-1, while the methyl group in the 4-position of the pyridyl ring resulted in a relative higher $K_{\text{SV}}^{\text{app}}$ value. Complexes with a fluoro or trifluoromethyl group at the 5-position of the pyridyl ring provided a little higher $K_{\text{SV}}^{\text{app}}$ value than that of the LSTP-1. It is clear that the quenching constant (the sensitivity toward O₂) of LSTP-7 ($K_{\text{SV}}^{\text{app}} = 0.102 \text{ Torr}^{-1}$) is much higher than those of other Pt(II)

complexes. This is probably due to the conjugated effect of an electron-withdrawing cyano (C≡N) group on the 5-position of pyridine ring. Although nitriles have attracted much attention due to their potential applications in laser frequency doubling integrated optics and optical communication [60,61], to the best of our knowledge, the present result is the first example of a nitrile compound used as a cyclometalating ligand for the O₂ sensing.

4. Conclusions

In summary, a series of luminescent Pt(II) complexes featuring functionalized hole-transporting TPA-based ligands were synthesized and fully characterized. The structure–property relationships were studied systematically. All complexes exhibit intense absorption bands with λ_{max} in a range of 533–596 nm. The HOMO and LUMO levels are little influenced by a methyl group at the 4, 5, 6-position or a fluoro group at the 5-position of the pyridyl ring. Introducing an electron-withdrawing group like cyano or trifluoromethyl group on the pyridine ring affects the LUMO level significantly, resulting in a marked decrease in energy gap and thus red-shifted emission. All complexes exhibited intense phosphorescence emissions at room temperature. These neutral and air-stable complexes were easily prepared, rendering good potential in luminescence oxygen sensors. Among them the complex LSTP-7 demonstrated the highest sensitivity toward the oxygen sensing, which is the first example of a nitrile compound used as a cyclometalating ligand for the efficient O₂ sensing. The present results disclose the color-tuning strategy for the design of novel Pt(II) complexes with good photoelectric performances for O₂ sensing.

Acknowledgment

The authors thank the financial support from the National Natural Science Foundation of China (21276043), and the Ministry of Education (the Program for New Century Excellent Talents in University).

Appendix A. Supplementary data

Supplementary data related to this article can be found at <http://dx.doi.org/10.1016/j.dyepig.2013.09.030>.

References

- Ishii T, Kaneko M. Photoluminescence of pyrenebutyric acid incorporated into silicone film as a technique in luminescent oxygen sensing. Analyst 1995;120(6):1633.
- Lakowicz JR. Principles of fluorescence spectroscopy. 2nd ed. New York: Kluwer Academic/Plenum Publishers; 1999.
- Gray JM, Karow DS, Lu H, Chang AJ, Chang JS, Ellis RE, et al. Oxygen sensation and social feeding mediated by a *C. elegans* guanylate cyclase homologue. Nature 2004;430(6997):317–22.
- Wolfbeis OS. Sensor paints. Adv Mater 2008;20(19):3759–63.
- Higgins C, Wencel D, Burke CS, MacCraith BD, McDonagh C. Novel hybrid optical sensor materials for in-breath O(2) analysis. Analyst 2008;133(2):241–7.
- Persson A, Gross E, Laurent P, Busch KE, Bretes H, de Bono M. Natural variation in a neural globin tunes oxygen sensing in wild *Caenorhabditis elegans*. Nature 2009;458(7241):1030–3.
- Wang Z, Chen T, Xu J. Gas and water vapor transport through a series of novel poly(aryl ether sulfone) membranes. Macromolecules 2001;34(26):9015–22.
- Quaranta M, Borisov SM, Kliment I. Indicators for optical oxygen sensors. Bioanal Rev 2012;4(2–4):115–57.
- Amao Y. Probes and polymers for optical sensing of oxygen. Microchim Acta 2003;143(1):1–12.
- Lu X, Winnik MA. Luminescence quenching in polymer/filler nanocomposite films used in oxygen sensors. Chem Mater 2001;13(10):3449–63.
- Huynh L, Wang Z, Yang J, Stoeva V, Lough A, Manners I, et al. Evaluation of phosphorescent rhenium and iridium complexes in polythionylphosphazene films for oxygen sensor applications. Chem Mater 2005;17(19):4765–73.

- [12] Han B-H, Manners I, Winnik MA. Oxygen sensors based on mesoporous silica particles on layer-by-layer self-assembled films. *Chem Mater* 2005;17(12):3160–71.
- [13] Vanderkooi JM, Wilson DF. Oxygen transport to tissue VIII. In: Langmuir IS, editor. New York: Plenum; 1986. p. 189.
- [14] Amao Y, Ishikawa Y, Okura I. Green luminescent iridium(III) complex immobilized in fluoropolymer film as optical oxygen-sensing material. *Anal Chim Acta* 2001;445(2):177–82.
- [15] Ji S, Wu W, Wu W, Song P, Han K, Wang Z, et al. Tuning the luminescence lifetimes of ruthenium(II) polypyridine complexes and its application in luminescent oxygen sensing. *J Mater Chem* 2010;20(10):1953.
- [16] Wu W, Cheng C, Wu W, Guo H, Ji S, Song P, et al. Tuning the emission colour of triphenylamine-capped cyclometallated platinum(II) complexes and their application in luminescent oxygen sensing and organic light-emitting diodes. *Eur J Inorg Chem* 2010;29:4683–96.
- [17] Wolfbeis O, Leiner MP, Posch H. A new sensing material for optical oxygen measurement, with the indicator embedded in an aqueous phase. *Microchim Acta* 1986;90(5–6):359–66.
- [18] Di Marco G, Lanza M, Pieruccini M, Campagna S. A luminescent iridium(III) cyclometallated complex immobilized in a polymeric matrix as a solid-state oxygen sensor. *Adv Mater* 1996;8(7):576–80.
- [19] Zhang H, Sun Y, Ye K, Zhang P, Wang Y. Oxygen sensing materials based on mesoporous silica MCM-41 and Pt(II)-porphyrin complexes. *J Mater Chem* 2005;15(31):3181–6.
- [20] Ma B, Djurovich PI, Garon S, Alleyne B, Thompson ME. Platinum binuclear complexes as phosphorescent dopants for monochromatic and white organic light-emitting diodes. *Adv Funct Mater* 2006;16(18):2438–46.
- [21] Suzuki S, Sugimura R, Kozaki M, Keyaki K, Nozaki K, Ikeda N, et al. Highly efficient photoproduction of charge-separated states in donor–acceptor-linked bis(acetylide) platinum complexes. *J Am Chem Soc* 2009;131(30):10374–5.
- [22] Zhao Q, Li F, Huang C. Phosphorescent chemosensors based on heavy-metal complexes. *Chem Soc Rev* 2010;39(8):3007–30.
- [23] Wu W, Xu X, Yang H, Hua J, Zhang X, Zhang L, et al. D–π–M–π–A structured platinum acetylide sensitizer for dye-sensitized solar cells. *J Mater Chem* 2011;21(29):10666.
- [24] Wu W, Zhang J, Yang H, Jin B, Hu Y, Hua J, et al. Narrowing band gap of platinum acetylide dye-sensitized solar cell sensitizers with thiophene π-bridges. *J Mater Chem* 2012;22(12):5382.
- [25] Xu XD, Zhang J, Yu X, Chen LJ, Wang DX, Yi T, et al. Design and preparation of platinum–acetylide organogelators containing ethynyl-pyrene moieties as the main skeleton. *Chem Eur J* 2012;18(50):16000–13.
- [26] Jiang B, Chen LJ, Xu L, Liu SY, Yang HB. A series of new star-shaped or branched platinum–acetylide derivatives: synthesis, characterization, and their aggregation behavior. *Chem Commun* 2013;49(62):6977–9.
- [27] Li ZY, Xu L, Wang CH, Zhao XL, Yang HB. Novel platinum–acetylide metallocycles constructed via a stepwise fragment coupling approach and their aggregation behaviour. *Chem Commun* 2013;49(55):6194–6.
- [28] Xu XD, Zhang J, Chen LJ, Zhao XL, Wang DX, Yang HB. Large-scale honeycomb microstructures constructed by platinum–acetylide gelators through supramolecular self-assembly. *Chem Eur J* 2012;18(6):1659–67.
- [29] Papkovskii DB, Yaropolov AI, Savitskii AP, Olah J, Rumyantseva VD, Mironov AF, et al. Fibre-optic oxygen sensor based on phosphorescence quenching. *Biomed Sci* 1991;2(5):536–9.
- [30] Xiang H, Zhou L, Feng Y, Cheng J, Wu D, Zhou X. Tunable fluorescent/phosphorescent platinum(II) porphyrin–fluorene copolymers for ratiometric dual emissive oxygen sensing. *Inorg Chem* 2012;51(9):5208–12.
- [31] Papkovsky DB, Ponomarev GV, Trettnak W, O’Leary P. Phosphorescent complexes of porphyrin ketones: optical properties and application to oxygen sensing. *Anal Chem* 1995;67(22):4112–7.
- [32] Papkovsky DB, O’Riordan TC. Emerging applications of phosphorescent metalloporphyrins. *J Fluoresc* 2005;15(4):569–84.
- [33] Wu W, Guo H, Wu W, Ji S, Zhao J. Long-lived room temperature deep-red/near-IR emissive intraligand triplet excited state (3IL) of naphthalimide in cyclometalated platinum(II) complexes and its application in upconversion. *Inorg Chem* 2011;50(22):11446–60.
- [34] Wang J, He C, Wu P, Wang J, Duan C. An amide-containing metal–organic tetrahedron responding to a spin-trapping reaction in a fluorescent enhancement manner for biological imaging of no in living cells. *J Am Chem Soc* 2011;133(32):12402–5.
- [35] Liang M, Xu W, Cai F, Chen P, Peng B, Chen J, et al. New triphenylamine-based organic dyes for efficient dye-sensitized solar cells. *J Phys Chem C* 2007;111(11):4465–72.
- [36] Su YZ, Lin JT, Tao Y-T, Ko C-W, Lin S-C, Sun S-S. Amorphous 2,3-substituted thiophenes: potential electroluminescent materials. *Chem Mater* 2002;14(4):1884–90.
- [37] Jou JH, Chen CC, Chung YC, Hsu MF, Wu CH, Shen SM, et al. Nanodot-enhanced high-efficiency pure-white organic light-emitting diodes with mixed-host structures. *Adv Funct Mater* 2008;18(1):121–6.
- [38] Tamoto N, Adachi C, Nagai K. Electroluminescence of 1,3,4-oxadiazole and triphenylamine-containing molecules as an emitter in organic multilayer light emitting diodes. *Chem Mater* 1997;9(5):1077–85.
- [39] He Z, Wong W-Y, Yu X, Kwok H-S, Lin Z. Phosphorescent platinum(II) complexes derived from multifunctional chromophores: synthesis, structures, photophysics, and electroluminescence. *Inorg Chem* 2006;45(26):10922–37.
- [40] Mak CSK, Pentlehner D, Stich M, Wolfbeis OS, Chan WK, Yersin H. Exceptional oxygen sensing capabilities and triplet state properties of Ir(ppy-NPh₂)₃. *Chem Mater* 2009;21(11):2173–5.
- [41] Liu C, Rao X, Song X, Qiu J, Jin Z. Palladium-catalyzed ligand-free and aqueous Suzuki reaction for the construction of (hetero)aryl-substituted triphenylamine derivatives. *RSC Adv* 2013;3(2):526–31.
- [42] Brooks J, Babayan Y, Lamansky S, Djurovich PI, Tsyba I, Bau R, et al. Synthesis and characterization of phosphorescent cyclometalated platinum complexes. *Inorg Chem* 2002;41(12):3055–66.
- [43] Ma B, Li J, Djurovich PI, Yousufuddin M, Bau R, Thompson ME. Synthetic control of Pt–Pt separation and photophysics of binuclear platinum complexes. *J Am Chem Soc* 2004;127(1):28–9.
- [44] Chassot L, Mueller E, Von Zelewsky A. *cis*-Bis(2-phenylpyridine)platinum(II) (CBPPP): a simple molecular platinum compound. *Inorg Chem* 1984;23(25):4249–53.
- [45] Laskar IR, Hsu S-F, Chen T-M. Highly efficient orange-emitting OLEDs based on phosphorescent platinum(II) complexes. *Polyhedron* 2005;24(8):881–8.
- [46] Hohenberg P, Kohn W. Inhomogeneous electron gas. *Phys Rev* 1964;136(3B):B864–71.
- [47] Frisch MJTG, Schlegel HB, Scuseria GE, Robb MA, Cheeseman JR. Gaussian 09. Revision A.1. Wallingford, CT: Gaussian Inc.; 2009.
- [48] Pommerehne J, Vestweber H, Guss W, Mahrt RF, Bässler H, Porsch M, et al. Efficient two layer leds on a polymer blend basis. *Adv Mater* 1995;7(6):551–4.
- [49] Zhou G, Wang Q, Wang X, Ho C-L, Wong W-Y, Ma D, et al. Metallophosphors of platinum with distinct main-group elements: a versatile approach towards color tuning and white-light emission with superior efficiency/color quality/brightness trade-offs. *J Mater Chem* 2010;20(35):7472.
- [50] Grushin VV, Herron N, LeCloux DD, Marshall WJ, Petrov VA, Wang Y. New, efficient electroluminescent materials based on organometallic Ir complexes. *Chem Commun (Camb)* 2001;(16):1494–5.
- [51] Tsuboyama A, Iwawaki H, Furugori M, Mukaide T, Kamatani J, Igawa S, et al. Homoleptic cyclometalated iridium complexes with highly efficient red phosphorescence and application to organic light-emitting diode. *J Am Chem Soc* 2003;125(42):12971–9.
- [52] Wolfbeis O, Narayanaswamy R. Optical sensors: industrial, environmental and diagnostic applications. Berlin, Heidelberg: Springer; 2004.
- [53] Wang Z, Chen T, Xu J. Gas transport properties of novel cardo poly(aryl ether ketone)s with pendant alkyl groups. *Macromolecules* 2000;33(15):5672–9.
- [54] Ji S, Wu W, Wu Y, Zhao T, Zhou F, Yang Y, et al. Real-time monitoring of luminescent lifetime changes of PtOEP oxygen sensing film with LED/photodiode-based time-domain lifetime device. *Analyst* 2009;134(5):958–65.
- [55] Leventis N, Rawashdeh A-MM, Elder IA, Yang J, Dass A, Sotiriou-Leventis C. Synthesis and characterization of Ru(II) tris(1,10-phenanthroline)-electron acceptor dyads incorporating the 4-benzoyl-N-methylpyridinium cation or N-benzyl-N-methyl viologen. Improving the dynamic range, sensitivity, and response time of sol–gel-based optical oxygen sensors. *Chem Mater* 2004;16(8):1493–506.
- [56] Yeh T-S, Chu C-S, Lo Y-L. Highly sensitive optical fiber oxygen sensor using Pt(II) complex embedded in sol–gel matrices. *Sens Actuators B* 2006;119(2):701–7.
- [57] Basu BJ. Optical oxygen sensing based on luminescence quenching of platinum porphyrin dyes doped in ormosil coatings. *Sens Actuators B* 2007;123(1):568–77.
- [58] Wang B, Liu Y, Li B, Yue S, Li W. Optical oxygen sensing materials based on trinuclear starburst ruthenium(II) complexes assembled in mesoporous silica. *J Lumin* 2008;128(3):341–7.
- [59] Zhou G-J, Wang Q, Wong W-Y, Ma D, Wang L, Lin Z. A versatile color tuning strategy for iridium(III) and platinum(II) electrophosphors by shifting the charge-transfer states with an electron-deficient core. *J Mater Chem* 2009;19(13):1872–83.
- [60] Brown HC, Okamoto Y. Electrophilic substituent constants. *J Am Chem Soc* 1958;80(18):4979–87.
- [61] Edelstein L, Stetz MA, McMahon HA, Londergan CH. The effects of α-helical structure and cyanlated cysteine on each other. *J Phys Chem B* 2010;114(14):4931–6.